GSA Data Repository 2019135

A geomorphological assessment of washload sediment fluxes and floodplain sediment sinks along the lower Amazon River

Edward Park[1] and Edgardo Latrubesse[1]

[1]Earth Observatory of Singapore and [3]Asian School of the Environment, Nanyang Technological University

Table of contents:

Table DR 1. Summary of *Q* and *SSSC* field data at gauge stations used in this study.

Station (*abbr.*/HYBAM station code)	River	Drainage area (10^3 km^2) [a]	Mean annual *Q* (m^3/s) [a]	*Q* data period (daily)	Field-*SSSC* data period/ sample size	Dominant geotectonic [e]
Fazenda Vista Alegre (*FVA*/15860000)	Madeira	1325	26,000	1967-2015	1997-2014/ 488	
Manacapuru (*MAN*/14100000)	Amazon	2148	105,000	1972-2015	1995-2014[c]/ 518	
Itacoatiara[g] (*ITC*/16030000)	Amazon	4280	165,000[b]	1972-2015	-	Andean foreland and lowland
Parintins[h] (*PAR*/16350002)	Amazon	4398	164,000[b]	1967-2015	-	
Obidos (*OBI*/17050001)	Amazon	4619	168,000	1968-2015	1994-2014[c]/ 558	
Monte Alegre[i] (*MAL*/virtual station)	Amazon	5320	177,000[b]	2000-2015	-	
Itaituba (*ITA*/17730000)	Tapajós	490	13,500	1968-2015	1997-2013[d]/ 316	Cratonic (shields)
Manaus[f] (*MAO*/14990000)	Negro	712	34,000	1970-2014	-	Cratonic
-Serrinha (*SER*/14420000)	Negro	280	17,000[b]	1967-2015	1996-2008[d]/ 239	Cratonic
-Caracarai (*CAR*/14710000)	Branco	125	3,000[b]	1967-2015	1996-2014[d]/ 500	Cratonic

[a] Dataset from Filizola and Guyot (2009) and Latrubesse et al. (2005); [b] Calculated in this study; [c] These field *SSSC* samples are used only for MODIS data calibration purpose; [d] For the black water tributaries, these field *SSSC* data is used for *Qwl* calculation; [e] Amazon Basin geotectonic settings classification based on hydrosedimentologic regimes by Latrubesse et al. (2017); [f] Due to backwater effect at the lower Negro, *Q* is not regularly measured at Manaus (Meade et al., 1991), thus we used *Q* and *SSSC* data at the two upstream gauge stations: Serrinha and Caracarai

to calculate washload discharge (*Qwl*). Discharge at *MAO* (Q_{MAO}) is calculated as the sum of *Q* at Jatuarana and Careiro subtracted by Q_{MAN} (Ronchail et al., 2006).; [g] *Qwl* at Itacoatiara (Qwl_{ITA}) is calculated as the sum of washload fluxes from *MAN* (Qwl_{MAN}), *MAO* (Qwl_{MAO}) and *FVA* (Qwl_{FVA}), assuming that the sedimentation over each reach in between *MAN* and Madeira confluence is minimal (discussed in Results section).; [h] Daily Q_{PAR} is estimated based on daily water level data available at Parintins using the rating curve generated using ADCP data (N=51) from HYBAM.; [i] We generated a virtual gauge station at Monte Alegre (*MAL*), where daily *Q* is estimated as the sum of Q_{OBI} and Q_{ITA}.

Text DR1. Methodological details

Hydrosedimentologic data at gauge stations

Daily water discharge (*Q*) and surface suspended sediment concentration (*SSSC*) data were supplied from the Hydrogeodynamics of the Amazon (HYBAM) (Table DR1). We used hydrological data from four gauge stations along the Solimões-Amazon River: Manacapuru (*MAN*), Itacoatiara (*ITC*), Parintins (*PAR*) and Obidos (*OBI*), and three lowermost stations from the major tributaries: Fazenda Vista Alegre (*FVA*) in Madeira River, Manaus (*MAO*) in Negro River, and Itaituba (*ITA*) in Tapajós River. A total of 2,619 *SSSC* samples processed across the gauge stations by HYBAM were used to calibrate with remote sensing data, and to calculate washload fluxes.

Surface water samples (SSSC) and grain size distribution lab analysis methods

We followed a similar protocol than HYBAM and Mertes et al. (1993) to collect surface water samples and to process suspended concentration data. A total of 121 Surface water samples were collected using 500 ml bottle along the river and the floodplain during two field campaigns: 40 samples in September 2015 and 81 samples in June 2016. Cellulose acetate membranes (0.45 μm) is used to filter sediments (Merck Millipore) and weighted after drying 24 hours to retrieve *SSSC*. Also, 23 buckets of surface water samples (20 liters) along the channel and in floodplain lakes were collected during 2016 field work to analyze the sediment grain size distribution of surface water. Collected bucket water samples were settled over 20 hours before removing 80% of the upper layer and then completely dried. We used laser particle scanner (Fritsch Analysette-22) to obtain the grain size distribution of each sample. All laboratory works were performed at the Geosciences Lab at the University of Texas at Austin.

Generating SSSC maps

Regionally calibrated regression models along the Amazon (i.e. *MAN* and *OBI*) are applied to the MODIS images to generate *SSSC* maps. The MODIS composite image, that is produced with the best quality pixels out of successive acquisition periods using constrained-view angle maximum value method (Huete et al., 2002) are efficient in generating spatially continuous maps in the Amazon Basin where frequent heavy cloud cover is present (Mertes and Magadzire, 2007). A total of 2,944 MODIS data (at every 8 days) were downloaded from USGS Earth Explorer and *SSSC* maps were created along the Amazon River reach including floodplain between Manacapuru and Monte Alegre (Park and Latrubesse, 2014). Further image processing methods including classification and water mask extraction, controlling pixel quality, and interpolating unqualified pixels can be found in Park and Latrubesse (2014). *SSSC* maps over both channel and floodplain enable quantitative assessments of the spatiotemporal distribution patterns of suspended sediments. Moreover, imaging of the water coverage over the levee complex and sediment plumes through the splay delta in the impeded rounded lakes in floodplain from remote sensing provides direct observation of the overbank diffusive processes. Inter-annual average *SSSC* map over the Amazon River was generated out of time-series *SSSC* maps, shown in Fig. 1. First, the maximum water extent on the floodplain is delineated that usually happens in early June. Within the maximum water extent, all the other images' pixels that don't reach this limit, was assigned the value of 0 (zero). Then, entire MODIS *SSSC* maps (with non-water pixel designated with a value of zero) are averaged, to produce a single image showing the average *SSSC* of the floodplain on annual basis.

Analyzing channel migration rates (1985-2015) using Landsat

Bank stability is an important factor in assessing sediment discharge of the river. Because if the river is laterally active (e.g. abandoning branches or generating new connections to the floodplain), the Amazon River's sediment discharge might be inter-annually variable due to the local controls on the transferences and storages of suspended sediments. For this, we assessed the channel migration rates (as channel-width per year, ch-w/yr) for the Amazon in between Manacapuru and Monte Alegre over 30 years (1985-2015). First, Amazon channel banks were digitized based on Landsat 5-7 images (30 m resolution at 100 m longitudinal spacing) during low water season at every 5 years interval. Then we generated difference polygons induced by erosion or deposition to calculate the average channel migration rates. Our calculated rates were compared to the published migration rates of the further upstream Amazon (Constantine et al., 2014) and other large tributaries of the Amazon (Latrubesse et al., 2017).

Calculation of Q_{wl} for each station

We analyzed the fine suspended sediment (washload in permanent suspension) fluxes (Q_{wl}) at eight *in situ* gauge stations from the main channel and tributaries (Fig. 1) based on an unprecedentedly large set of remote sensing (every 8-days interval throughout 2001-2015, N=2,944) and gauge station data (1994-2014, N=2,619). The 2,944 8-day composite MODIS data (MOD/MYD09Q1, L3) covering the entire middle-lower Amazon (h11v09 and h12v09) were used to obtain *SSSC* at gauge stations since 2000. The estimated washload fluxes were verified by field measurements (2015-2016) of water discharge, surface suspended sediment concentration and grain size distribution (as mentioned above) from the channel and floodplain.

Published regionally field-calibrated models were separately applied to three gauge stations: *MAN* and *OBI* by Park and Latrubesse (2014), and *FVA* by Villar et al. (2013) and Latrubesse et al. (2017) (Table DR2), and time series *SSSC* maps were generated.

Qwl of the Negro River at *MAO* was estimated as the sum of *Qwl* at Serrinha and Caracarai, while *Qwl* of Tapajós River was calculated at Itaituba (*ITA*) station (Fig. 1). Along both black water tributaries, *Q* and *SSSC* data have been sufficiently collected by National Water Agency of Brazil (ANA) and are available at HYBAM since the 1990s to calculate relevant *Qwl* annual discharges. Based on *Qwl* in 8-day intervals, monthly and annual *Qwl* were computed. Floodplain sediment storage along the lower Amazon River in between *MAN* and *OBI* were calculated as differences between the sum of *Qwl* at *MAN*, *MAO,* and *FVA*, and *Qwl* at *OBI* (as in Filizola and Guyot, 2009).

Since *Q* data were not monitored at PAR, we developed a rating curve based on daily water level data and ADCP measurements (N=51) based on HYBAM database (Fig. DR5). At *PAR*, the reach is stable with Cenozoic sedimentary rocks on the right bank and stable levee complex on the left bank. The channel is highly stable with 0.0032 ch-w/yr calculated over 60 km reach around *PAR* which is smaller than the entire Amazon River main channel (0.01 ch-w/yr) (Latrubesse et al., 2017), indicating that the levee around *PAR* is very stable and have been persistent over decades. For the final *Q* at *PAR*, discharges of two local branches were added, because PAR station is located at the middle of these branches. First one is Parana do Ramos, an atypically long branch where we obtained the ADCP survey data collected on March 2nd, 2001 from a HYBAM report (Kosuth et al., 2001). Using the cross-section area (10,223 m^2), velocity (0.794 m/s) from the ADCP data, and estimating *SSSC* from our MODIS time series at the same location of ADCP transect survey, we calculated the annual *Qwl* of the Parana do Ramos. Annual *Qwl* for another smaller branch at the opposite side of the Parintins gauge station was estimated using the width-depth ratio (*w/d*) of other geomorphologically similar branches. We used *w/d* of a typical branch in Madeira River (reach 3 in Guo (2017)'s Fig. 4.28) with similar sinuosity, confined with cohesive banks with high stability (both branches showed almost no migrations over the 40 years since 1975), incised in the floodplain and showing similar spatial scale. Given that field information on the branch is lacking, we consider that this *w/d* approach as the best possible method because both branches showed almost no bank line changes over the different season. We used the velocity of the Madeira branch as well, i.e. 0.85 m/s to calculate *Qwl* of the branch on the other side of the river from Parintins. Locations of both branches around Parintins are shown in Fig. DR5.

Downstream of Obidos, gauge stations are lacking in the Amazon River due to the tidal effect. From geomorphologic and sediment budgetary perspective, this might be problematic to estimate the total *Qwl* export of the basin to the ocean. Because vast floodplain system of the Amazon River ends even ~250 km further downstream of Obidos (Reach 4), around Monte Alegre (*MAL*) (Fig. 1) and that Nittrouer et al. (1995) estimated about 30% of suspended sediment could be further deposited in the reach between Obidos and mouth. Moreover, it has been reported that about 20 Mt of fine sediment from the Amazon River is deposited at rias valleys of Tapajós and Xingu Rivers annually (Fricke et al., 2017). Downstream *MAL* are terraces dominated older riverine landscapes, where we assume that the sediment loss to floodplain is negligible.

At *MAL*, Q is estimated as a sum of Q_{OBI} and Q_{ITA}. We acknowledge that this can result in a crude estimation of discharge, mainly due to the backwater effect from the ocean (Kosuth et al., 2009) and also the channel-floodplain connectivity in *OBI-MAL* reach where their storage capacities are not well-known. We refined Q_{MAL} based on our knowledge on channel-floodplain connectivity characteristics around Obidos. Previously, we found that at Obidos Q loss due to floodplain storage during the discharge rising phase each year is ≈7.6% less than that of the discharge estimated by the rating curve (Park, 2017). We applied same proportional loss to the discharge estimated at *MAL* because the size and geomorphic style of floodplains are similar.

Floodplain geomorphic mapping and identifying overbank diffusion thresholds

When mapping the floodplain extent, we adopted the geomorphic definition of floodplain (Latrubesse and Park, 2017) that includes older geomorphic units of alluvial materials those are not always inundated through typical seasonal flooding (Iriondo, 1982). The width of the floodplain is measured as a line perpendicular to the Amazon channel centerline touching each limit. At flood stage, overbank diffusive processes happen after the water stage exceeds the bank's height. Therefore, information on bank heights integrated with our field observations provide clues on the timing and the location of these processes, which will also illuminate identifying and characterizing the sediment sinks along the Amazon floodplain with different geomorphic styles (Park and Latrubesse, 2017). We conducted field surveys between August 25th and September 5^{th,} 2015 and June 24th and July 6^{th,} 2016 to identify different inundation conditions along the levee complex along the lower Amazon River reach in between Negro confluence and Monte Alegre (≈850 km). We also used vegetation removed SRTM DEM (O'Loughlin et al., 2016) to extract bank elevations at every 90 m longitudinal interval to assess the bank height distribution along the lower Amazon reach.

Geomorphologic Glossary

The fluvial belt of the Amazon River is a complex of Quaternary sedimentary units of different ages and formation conditions. The main Holocene units are the impeded floodplain and the channel-dominated floodplain as defined by Latrubesse and Franzinelli (2002) and Latrubesse (2012).

Channel-dominated floodplain (CDF): it is a complex mosaic of fluvial forms, including the active anabranching pattern of the Amazon: main channel and branches, active sandbars, islands, levees, scroll-dominated plains, abandoned fluvial belts, and related lakes (island lakes, scroll lakes, etc). This unit experiences partial recycling (deposition and erosion) by the present channel and suspended sand can be deposit and resuspended from these composite landform's mosaic.

*Impeded floodplain (IFP)***:** it is a widespread unit characterized by a very flat surface and round or irregularly shaped lakes where floodplain drainage is poorly developed and connected. The IPF is only partially affected by the present river floods, and some areas act as active sediment sinks of fine deposits. Wash load can be dominantly transferred to certain sectors of the IFP by overbank and, secondarily, by channelized floodplain flow generated from the main channel flowing toward lakes where still water sedimentation happens. Sandy supply to the IFP is very limited and sourced by small floodplain channels that originate in the lower Amazon main channel and branches, creating splays and deltas into the impeded floodplain lakes. Although some of these lakes are connected to the main system, many are isolated or can be only connected during large floods. The IFP resembles local flood basins formed by grey to grey-green muddy sediments. Orange of yellow bioturbated mottled sediments and intercalated layers of muddy sands in the delta lobes are also found.

*Water Saturated Floodplain (WSFP)***:** Large areas of the IFP in the lower Amazon river can store large volumes of Amazon channel sourced waters during the year. The flat relief, local tropical rainfall, a high water table, seepage, and flow inputs by local tributaries, contribute to sustaining large areas of lakes and ponds even when the Amazon River is at low water stage. The IFP relief is at a relatively lower elevation than the top of the levees and other landforms of the

CDF that confine the channel. It allows the floodplain maintenance of pounding water and large areas of water-saturated soils during the whole year, and the floodplain can be classified as a "water saturated". The level and spatial distribution of the channel-floodplain hydrological connectivity is controlled not only by the hydrological regime but also by the geomorphological composition of the floodplain (Mertes, 1997; Park and Latrubesse, 2017).

Geomorphologic Style: Reaches of a river with a characteristic character and behavior (form and function) (Brierley and Fryirs, 2013). At a certain reach, the geomorphologic style is the result of the combination of three main factors: fluvial planform and related landforms, the hydro-geomorphologic mosaic of the floodplain, and bed materials.

SSSC data availability and model validation

Annual temporal coverage (data availability) of MODIS data surpasses the field collected *SSSC* data by 20% at *FVA* to 42% at *OBI* over 15 years (2001-2015) (Fig. DR2a). Sufficient *SSSC* data coverage is crucial in calculating *Qwl*, especially in a river with strong hydroclimatic seasonality like the Amazon. Cross-validation results of MODIS-driven *SSSC* with HYBAM data also yielded high R^2 over gauge stations from different rivers (overall R^2>93, total N=932 field samples, Fig. DR2b). Additionally, estimated *SSSC* over channel and floodplain (far away from gauge stations), were further validated with *SSSC* samples collected in 2015 (N=33) and 2016 (N=51) field works. Since grain size distribution of surface sediments might affect the surface reflectance, we analyzed the surface water samples collected both in Madeira and Amazon River (Fig. DR3). We confirmed that all surface suspended sediments those were collected close to peak discharge period were exhaustively silt and clay with almost no sand, conforming to the previous observations that washload as a predominant particle type over water surface in the

Amazon River (Filizola and Guyot, 2009; Mertes et al., 1993). Methodological details are summarized as a flowchart in Fig. DR1.

Table DR2. MODIS calibration models to estimate *SSSC* used in this study.

Calibrated at (gauge station)	Model	RMSE (mg/l)[a]	R^2	Sample size	References
Manacapuru	$SSSC=27.05\cdot e^{7.83\cdot R1}$	6.2	0.88	232	Park and Latrubesse (2014)
Porte Velho[c]	$SSSC=1020\cdot(R2/R1)^{2.94}$ (Dec-Jul)	34.1	0.92	282	Villar et al. (2013)
	$SSSC=355.3\cdot(R2/R1)^{1.39}$ (Aug-Nov)	28.9	0.81	105	Latrubesse et al. (2017)
Obidos	$SSSC=649.99\cdot R1+3.42$ (Dec-Jun)	9.8	0.83	106	Park and Latrubesse (2014)
	$SSSC=631.68\cdot R1+1.55$ (Jul-Nov)	6.5	0.79	207	

R1 and *R2* denote reflectance and band 1 and 2, respectively.

[a] Root mean square error calculated as cross-validation from original field data from HYBAM.

[b] Calculated as mean annual values from MODIS-estimates (2001-2015).

[c] Models calibrated at Porto Velho are used to estimate *SSSC* at Fazenda Vista Alegre (*FVA*), because there is no major inputs or loss of sediment downstream from Porto Velho until *FVA*.

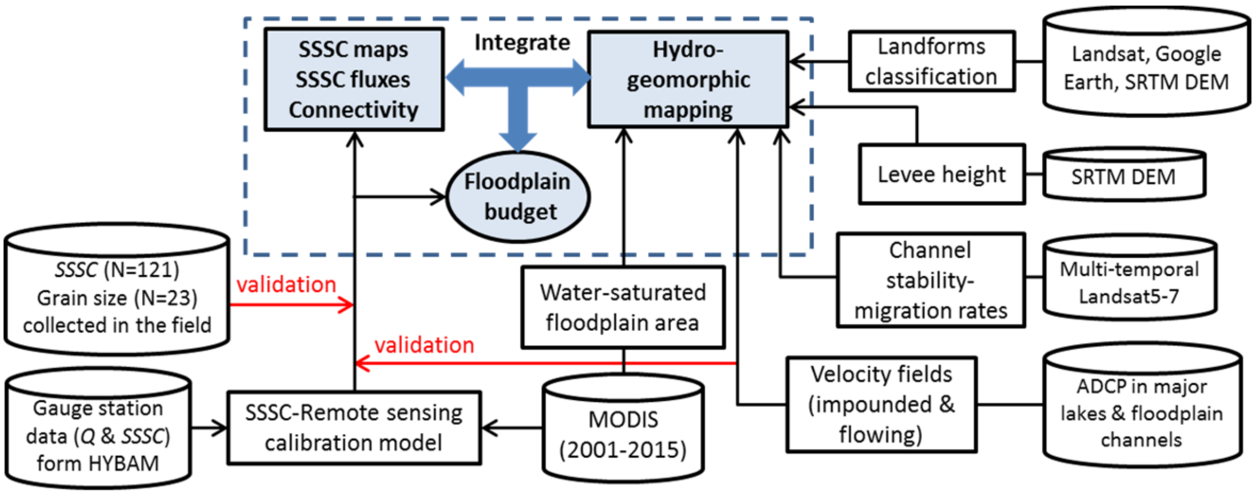

Fig. DR1. (a) A flowchart presenting methodological details developed in this study to assess the spatiotemporal distribution of sediments, sediment discharge, and floodplain budgets, within geomorphologic context.

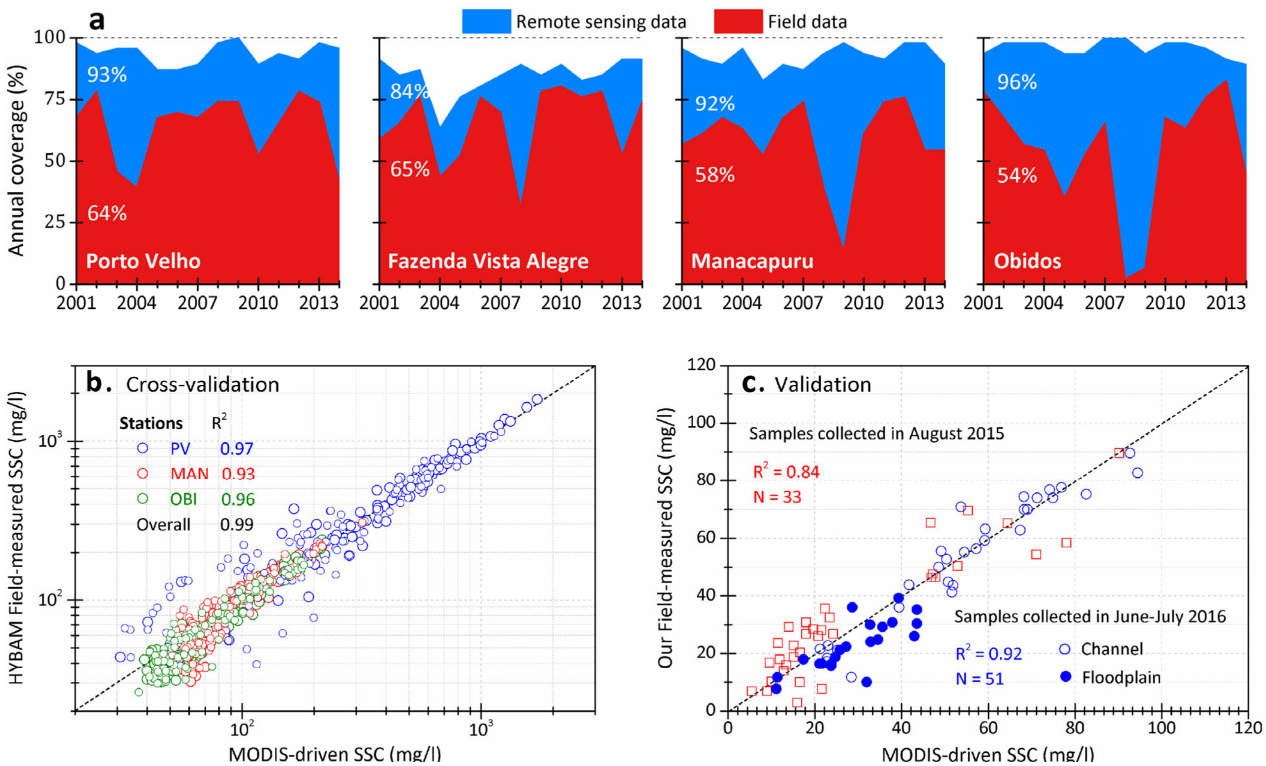

Fig. DR2. (a) Comparison of annual temporal coverages (data availability) between remote sensing and field data necessary to calculate the annual sediment fluxes (*Qwl*). Since MODIS data product is available at every 8 days interval, the annual coverage (blue) is calculated as a portion of the available scenes out of total 46 scenes per year. Similarly, HYBAM follows protocol to collect field SSC data at each gauge station on every 1st, 10th, and 20th days in of the month. Thus, the annual field data coverage (red) is calculated as the number of available field samples out of 36 total possible samples per year. Average annual temporal coverage values over 14 years (2001-2014) are also given. Martinez et al. (2009) explained the lower temporal coverage and irregular variability of field data could be due to variability in sampling location, operator reliability or loss of samples. (b) Cross-validation results of the SSC-reflectance calibration models used in this study (Table DR2) with HYBAM field SSC data and (c) additional validation results using our field SSC data collected during falling and peak limbs of 2015 (reach in between Manaus-Madeira confluence) and 2016 (reach in between Manaus-Monte Alegre). 2016 collected samples are separately plotted as channel (including branches) and floodplain. Samples collected in floodplain channels and black water tributaries are excluded.

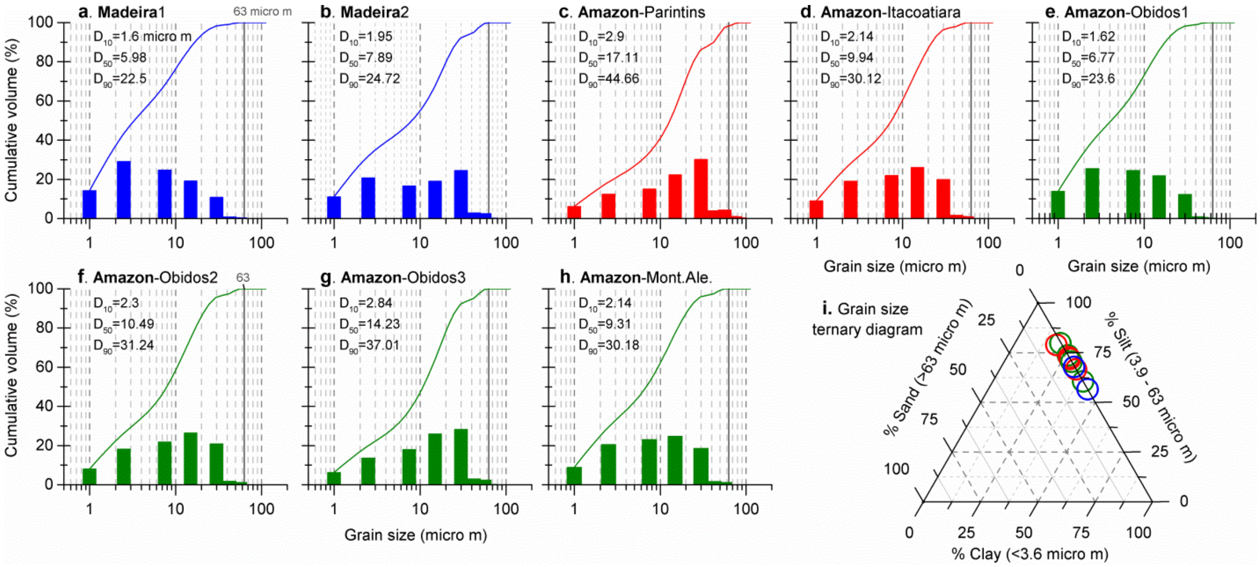

Fig. DR3. Grain size distribution results of the suspended sediment samples collected using 20 liter buckets during June-July field work in 2016. Locations of the samples: (a) -3.420947°, -58.788019°; (b) -3.503443°, -58.88593°; (c) -2.57016°, -56.608162°; (d) -3.157276°, -58.448858°; (e) -1.938752°, -55.504502°; (f) -1.940992°, -55.503997°; (g) -1.941706°, -55.510791°; (h) -2.462679°, -54.548152°.

Text DR2. Washload fluxes calculations at gauge stations

Washload transferences to the floodplain during floods

The water stages for hydrological connectivity between the channel and floodplain vary for each reach, and it is mostly a function of the geomorphic complexity of the floodplain, but in general, flood water stages are not higher than a few meters above the top of the highest levees (Park and Latrubesse, 2017). For example, in Obidos, the water stage range between the channel-floodplain connectivity level (overbank point) and the water level at flood peak is about 4 m. Mertes et al. (1996) also observed that the freeboard around Parintins was ≈1.5 m based on data from 1971-1977 field surveys.

Our assessments on floodplain deposition were based on washload fluxes at gauge stations (Text DR2 and Fig. 1) because washload is transferred to the floodplain during the floods by overbank while the input of sandy sediments is very limited. The absence of sand in the upper levels of the water column was earlier registered in Obidos by Meade (1985a). More recent studies of vertical profiles of *SSSC* in the Amazon River channel at Manacapuru, Foz Madeira (immediately upstream from the confluence) and Obidos during March and June (rising-peak), showed a homogeneous vertical distribution of suspended sediment concentration from the surface to approximately 10 m in depth where silt and secondarily clay, are the dominant sediment fraction (Bouchez et al. (2011). Our grain size distribution analyses from the surface water samples collected at the river surface in Itacoatiara, Parintins, Obidos and Monte Alegre, and in large floodplain lakes along the Amazon also confirmed the lack of sandy materials at overbank stages and the only presence of fine suspended sediments in the floodplain (Figs. DR3 and 6). The dominant grain size in all the samples is silt. Thus, based on all the data above we claim that fine washload is the predominant grain size transferred from the channel to the floodplain during floods in the lower Amazon.

Washload fluxes at gauge stations

Six of the stations from white water-muddy rivers (*MAN*, *FVA*, *ITC*, *PAR*, *OBI* and *MAL*) are important because they account for most of the suspended sediment transport of the Amazon Basin (Fig. DR4). Among these, we particularly focused on the three *in-situ* gauge stations: *MAN*, *OBI* and *FVA* where daily discharge data are collected, and weekly *SSSC* data are estimated from field-calibrated remote sensing models (Table DR1 and 2). These three gauge stations are used as "anchors" of washload discharge and floodplain budget calculations in this study where values can be considered more precise than other stations due to the robustness of the data (thus without any assumptions). Therefore, in this section, we present the results of these three gauge stations in advance of others.

The *MAN* station on the lower Solimões River (upstream from the confluence with the Negro River), which the upstream area occupies ≈35% of the Amazon Basin represents the water drainage and sediment loads of the Andean-forelands characterized by high sediment yields (Latrubesse and Restrepo, 2014). Mean annual *Q* at *MAN* is around 101,000 m^3/s which is close to half of the total Amazon River *Q* at *OBI* (Molinier et al., 1995). Our estimated inter-annual average *Qwl* at *MAN* is 299 Mt/yr calculated over 15 years (2001-2015).

Madeira River is the largest tributary of the Amazon in basin size (≈25% of the Amazon Basin), discharge and also sediment loads. *FVA* is the lowermost gauge station on Madeira integrating over 95% of its basin area. Hydrological and sedimentological regimes in Madeira are, in general in phase. For example, mean monthly *SSSC* and *Qwl* are normally the lowest during August to

October when *Q* is also the lowest of year, presenting a huge seasonally varying contribution of washload to the Amazon River. Our estimated total annual *Qwl* of the Madeira River at *FVA* is 174 Mt/yr.

OBI is the lowermost station of the Amazon River, that encompasses ≈80% of the Amazon Basin (Filizola and Guyot, 2009). The station is also considered the lowermost station not affected by the tidal effects (Kosuth et al., 2009). Seasonal patterns of the *SSSC* and *Q*, and in turn *Qwl* are altered from *MAN* mainly due to the influence from the two largest tributaries: Negro and Madeira Rivers. Lowered mean monthly *SSSC* during August-September at *OBI* compared to *MAN* should be the most obvious change (Fig. DR4). During this period, Amazon River's *Q* contribution from the Negro and Madeira Rivers are at their highest and the lowest, respectively. Increased black water input from the Negro and low input of muddy water from Madeira during this season results in dramatic decrease in *SSSC* at *OBI*. We estimated annual washload flux at *OBI* as 403 Mt/yr. The maximum *Qwl* discharging month has been shifted from January at *MAN* to March at *OBI* (64 Mt/month), which coincides the *Qwl* peak at *FVA*. At MAL (a virtual station), *Qwl* is calculated as 358 Mt with similar seasonal *SSSC* and *Q* behaviors with *OBI*.

Annual *Qwl* at *ITC* is computed to be 478 Mt, by summing *Qwl* at *MAN*, *FVA,* and *MAO*. Loss of *Qwl* over a reach in between Manacapuru and Madeira confluence is assumed to be negligible because development of impeded floodplain in this reach is limited and the sedimentary rocks (Cretaceous Alter do Chão Formation) confine left bank of the river (Latrubesse and Franzinelli, 2002) (Fig. 1). *SSSC* were not calculated at *ITA* due to the incomplete mixing of the different upstream water sources (i.e. Amazon, Negro, and Madeira Rivers) (Park and Latrubesse, 2015).

PAR divides the reach 2 and 3. At *PAR*, we developed a rating curve based on daily water level data and ADCP measurements (N=51) based on HYBAM database (Fig. DR5). At *PAR*, the reach is stable with Cenozoic sedimentary rocks on the right bank and stable levee complex on the left bank. The channel is highly stable with 0.0032 ch-w/yr calculated over 60 km reach around *PAR* which is smaller than the entire Amazon River main channel (0.01 ch-w/yr) (Latrubesse et al., 2017), indicating that the levee around *PAR* is very stable and have been persistent over decades. Annual *Qwl* at *PAR* is estimated at 453 Mt.

Washload fluxes are also calculated in the two black water tributaries along the Amazon River: Negro and Tapajós Rivers (SI Figure 1). In these rivers, monthly and annual *Qwl* are estimated solely based on field data because *SSSC* could not be estimated efficiently from remote sensing over black waters (Park and Latrubesse, 2015). At the three stations used to calculate *Qwl*, HYBAM have already collected sufficient *Q* and *SSSC* data over time to relevantly estimate the annual washload budgets (Figure 1 and Table 1). In *MAO*, *Q* and *SSSC* data are not regularly collected and only available episodically, due to the backwater effect (Meade et al., 1991). Hence we calculated *Qwl* individually at the two upstream stations: Serrinha (*SER*) on Negro River and Caracarai (*CAR*) on Branco River (a tributary of Negro). They were summed up to retrieve the *Qwl* of Negro River at *MAO* assuming that the sediment loss to the floodplain will be minimal downstream from the two stations. Although *Qwl* budgets of these black water tributaries were very low as they drain dominantly cratonic regions, they show distinct seasonal variations with the highest *Qwl* discharges during June-July and February for the Negro and Tapajós Basins, respectively. Annual *Qwl* of Negro and Tapajós Rivers are calculated as 5.4 and 4.1 Mt/yr, respectively. All annual Qwl estimated in this study is summarized in Table DR3.

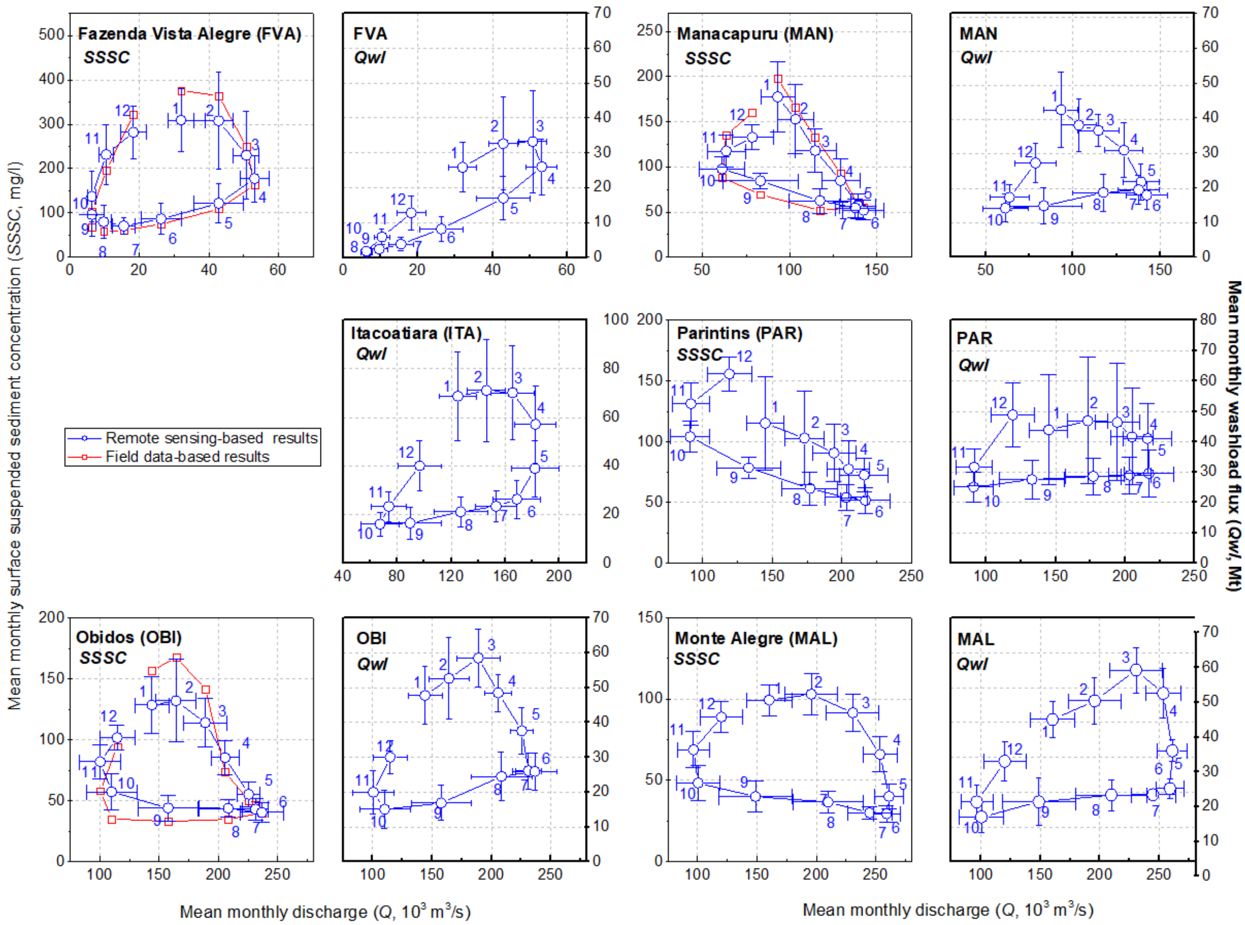

Fig. DR4. Seasonal variability of surface suspended sediment concentration (*SSC*, left) and washload fluxes (Q_{wl}, right) in relation with monthly water discharge are plotted at five major gauge stations along the white water rivers studied in this paper: Fazenda Vista Alegre (*FVA*), Manacapuru (*MAN*), Parintins (*PAR*), Obidos (*OBI*) and Monte Alegre (*MAL*). Field data-based calculations of *SSSC* and *Qwl* are also provided (red) using every available field data from HYBAM, which presents high correlations with our remote sensing-based estimates. Monthly average and variability (standard deviation) of sediment and discharge values are plotted to announce their seasonal tendency and visually enhance the comparison between months. Numbers in plots indicate month.

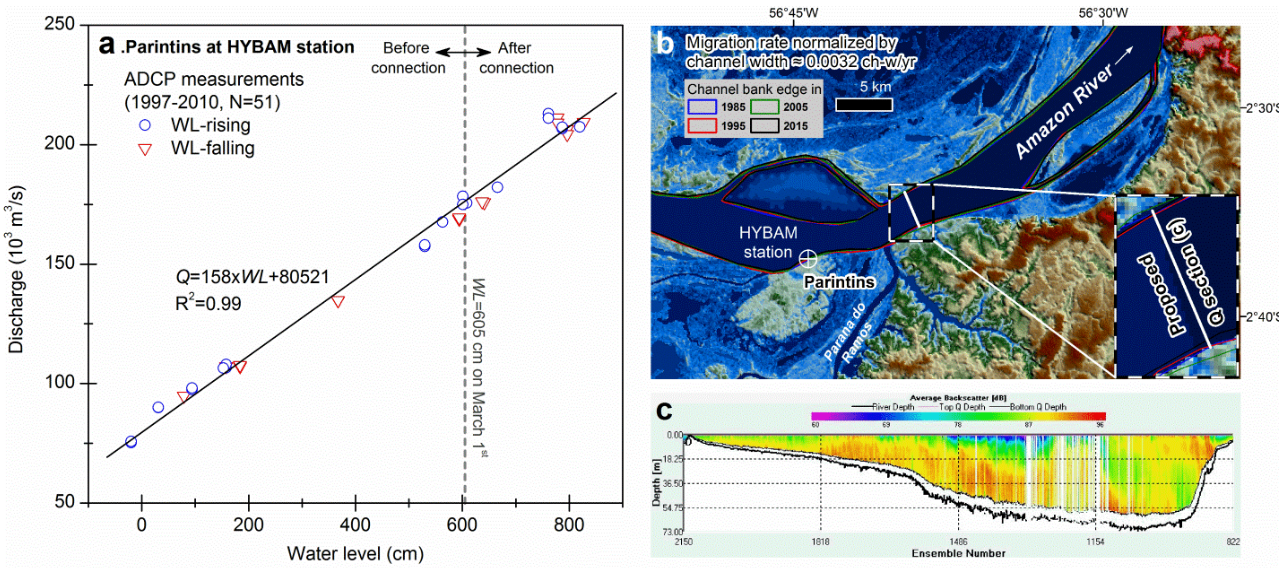

Fig. DR5. (a) ADCP Q data point (N=51 after filtering from the 106 original raw data, using the filteting protocol described in Park (2017). (b) HYBAM station at Parintins (code: 16350002, -2.63333°, -56.75195°) and ADCP Q section that we measured in the field. Average channel migration rate of the ~60 km reach shown in the map over 30 years (1985-2015) is 12 m/yr, average channel width in this reach is 3.8 km, and the normalized migration rate is 0.0032 ch-w/yr. The background is SRTM DEM. (c) ADCP transect collected on June 28th, 2016 (Q=205·10^3 m^3/s) shown in b.

Table DR3. Summary of inter-annually (2001-2015) averaged annual *Qwl* estimated in this study

	Qwl (Mt)	
Station (code)	Max. month (budget)/Min.	Annual *Qwl*
FVA	Mar (33)/Sep (1.5)	174
MAN	Jan (43)/Oct (14)	299
ITC	Feb (71)/Oct (15)	478
PAR	Feb (56)/Oct (18)	453
OBI	Mar (58)/Oct (15)	403
ITA	Feb (0.6)/Sep (0.1)	4.1
MAL	Mar (55)/Oct (13)	358
MAO	Jul (0.8)/Dec (0.2)	5.4
-SER	Jul (0.4)/Dec (0.2)	3.2
-CAR	Jul (0.4)/ Feb (0.04)	2.2

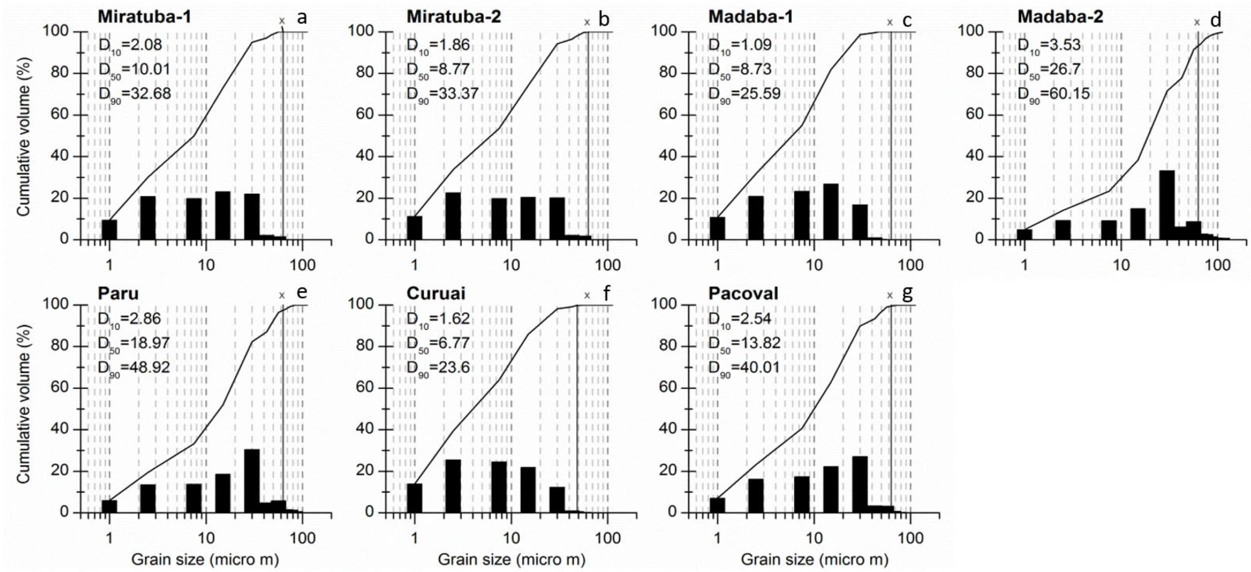

Fig. DR6. Grain size distribution results of the suspended sediment samples collected using 20 liter buckets in the Amazon River floodplain during June-July field work in 2016. Location of the floodplains is in Fig. 1. Locations of a to g: 3°13’57.03”S, 58°17’19.16”W; 3°14’47.33”S, 58°20’41.76”W; 2°16’43.22”S, 56°26’0.44”W; 2°17’1.23”S, 56°29’54.22”W; 1°52’59.27”S, 55°44’33.62”W; 2°8’16.31”S, 55°21’28.27”W; 2°17’50.80”S, 54°39’5.46”W.

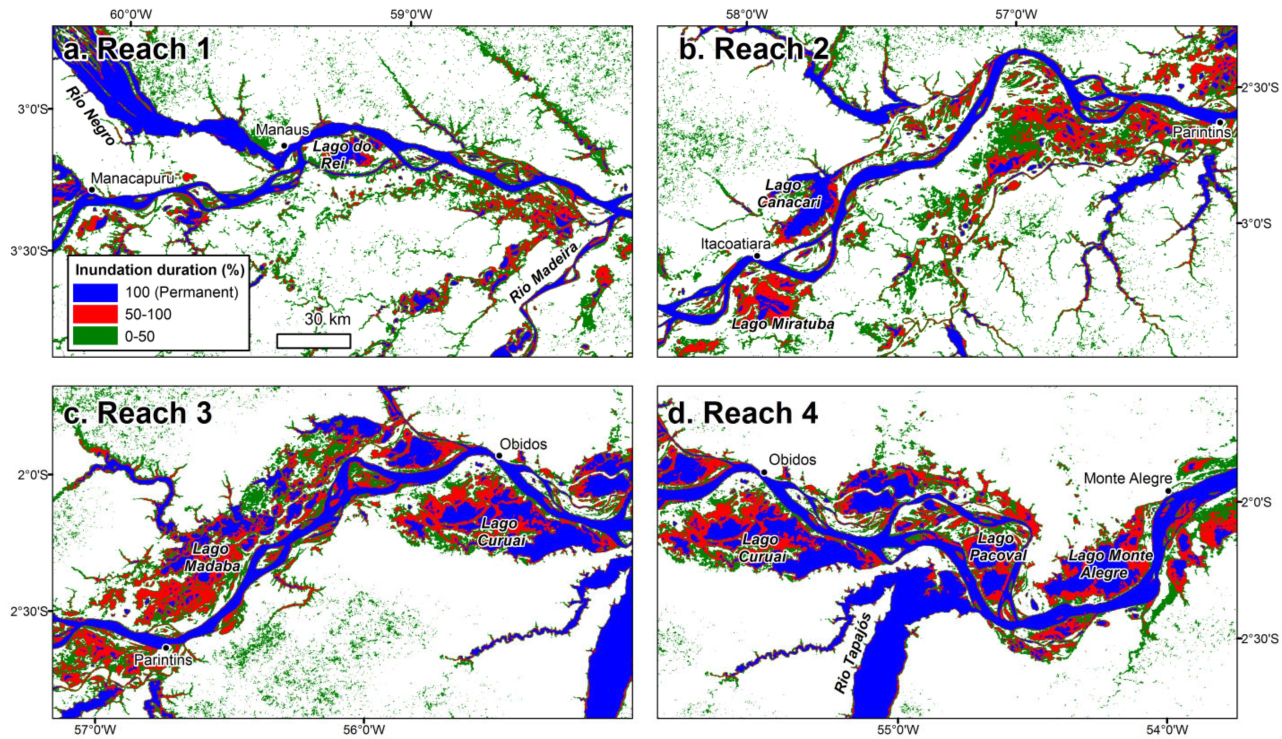

Fig. DR7. Inundation frequency (0-100 %) map along the study reach of the Amazon (Reach 1-4). All inset maps are in the same scale. Calculated using MODIS water mask over 15 years (2001-2015).

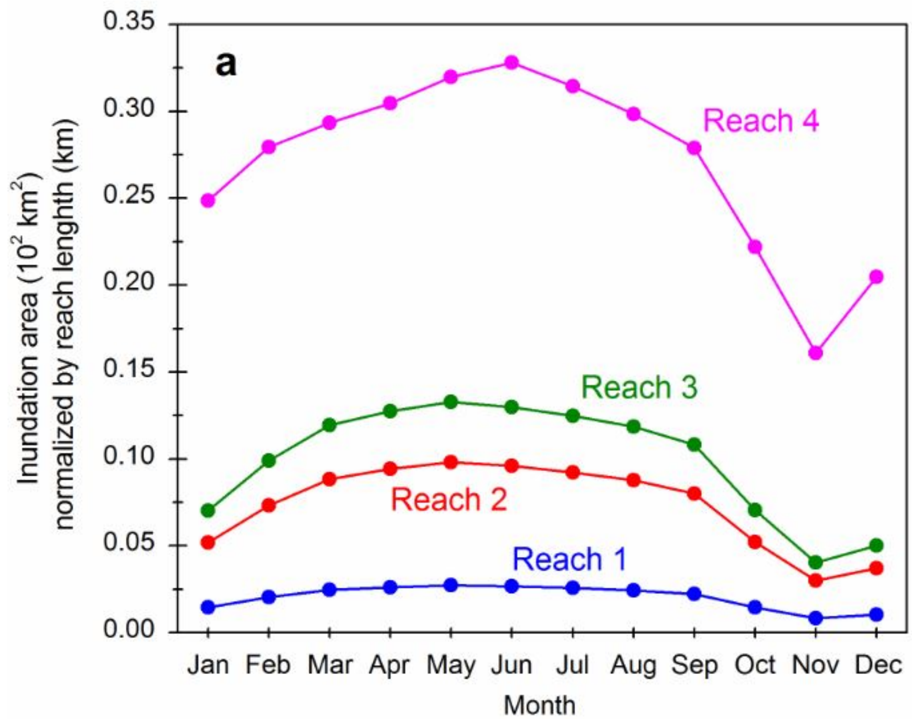

Fig. DR8. Total inundated area of each month for each unit is divided by total length of the reach, in order to derive area (km^2) per unit km that enables the comparison between reaches.

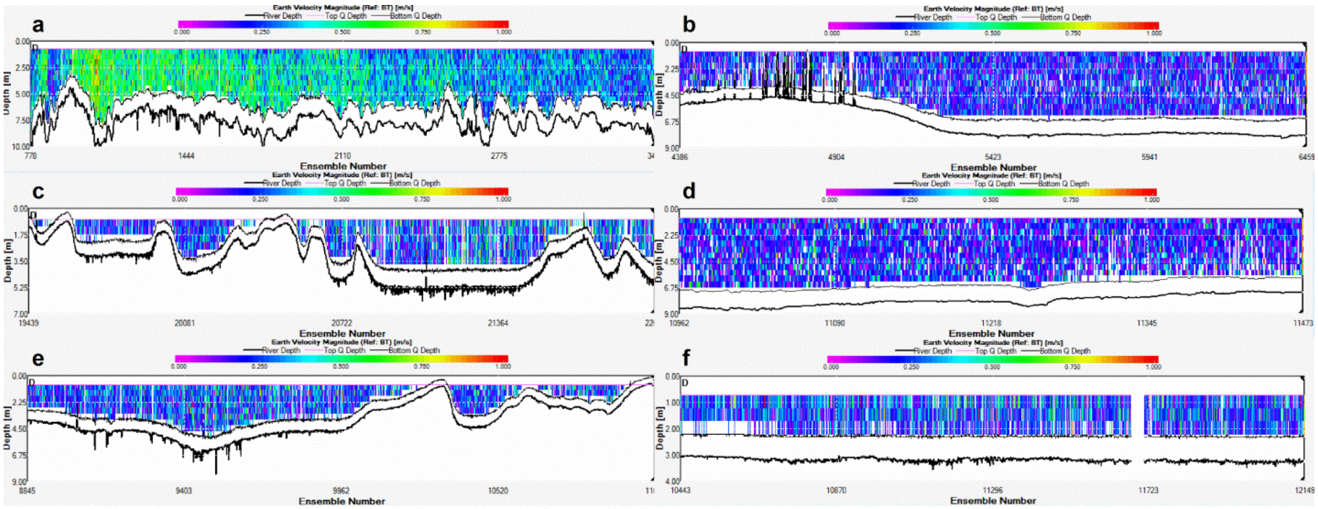

Fig. DR9. Collected ADCP profiles in the floodplain lakes along the Amazon during June 28th-July 6th, 2016. Floodplain lakes: (a) Miratuba, (b) Canacari, (c) Madaba, (d) Paru, (e) Curuai, and (f) Monte Alegre. Collected parameters are organized in Table DR4. Based on our velocity profiles collected in different floodplain lakes using ADCP around peak discharge season, impounded waters in floodplain were practically stagnant and not capable of keeping fine sediments in suspension or in producing resuspension. The depth-averaged velocities measured in different floodplain lakes (N=6) ranged from 0.022 to 0.186 m/s with an average velocity of entire floodplain around 0.12 m/s (Fig. DR9 and Table DR4). The surface temperature of these impounded lakes can become high as 32.78 or 31.42 °C in Canacari and Paru Lakes, respectively due to relatively long residence time, while it remained relatively cooler (28.06 °C) in the Amazon River around Obidos on similar dates (Table DR4).

Table DR4. Summary of ADCP data collected in floodplain along the lower Amazon in Fig. DR9.

Reaches	Floodplain lakes	Date	Survey length (m)	Average velocity (m/s)	Average depth (m)	Temperature (°C)
Reach 2	Miratuba	June 28th, 2016	3620.8	0.173	8.99	29.26
	Canacari	July 6th, 2016	1554.7	0.071	7.98	32.78
Reach 3	Madaba	July 4th, 2016	1903.4	0.123	5.21	29.86
	Paru	June 28th, 2016	546.7	0.022	7.17	31.42
Reach 4	Curuai	July 4th, 2016	1514.9	0.117	0.9	29.76
	Monte Alegre	July 2nd, 2016	1155.7	0.186	3.18	30.48

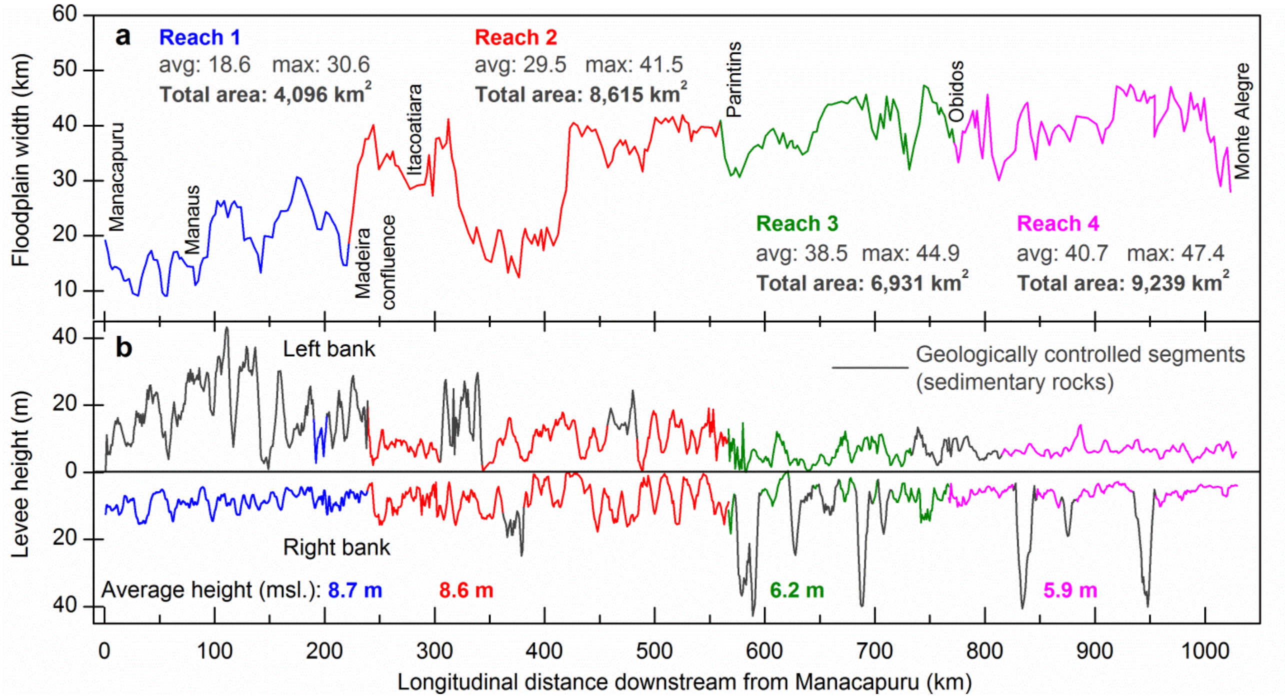

Fig. DR10. (a) Floodplain width and (b) bank height longitudinally downstream along the lower Amazon are mapped. Width of floodplain is not only related to the channel lateral activity and inundation dynamics of the river, but also to the structural features of the region. In Reach 1, neotectonic lineaments those are generally in NE-SW and E-W directions confining the fluvial belt are documented by Latrubesse and Franzinelli (2002). They mention that the fluvial belt can be locally narrow or wider oscillating between 7 to 20 km controlling the location and appearance of the alluvial plain in this region. In Reach 2-4, floodplain lies over "trough" confined by Guyana and Brazilian shields,however the fluvial belt becomes larger as well as floodplain extents. Levee height is corrected for the channel slope (2 cm/km) and geologically controlled segments are excluded in the calculation of average heights for each reach.

Table DR5. Floodplain morphometric characteristics of the reaches.

	Longitudinal length (km)	Average width (km)	Average bank height (m) [a]	Total floodplain extent (km^2)	Total Inundated area (TIA, km^2/km)[b]	Area flooded by river (FR, km^2/km)[b]	Impeded floodplain area (km^2/km)[b]
Reach 1	242	18.6	8.7	4,096	16.9	11.5	4.5
Reach 2	325	29.5	8.6	8,615	26.5	19.4	17.4
Reach 3	200	38.5	6.2	6,931	34.7	28.4	24.5
Reach 4	262	40.7	5.9	9,239	35.3	30.7	27.2

[a] calculated from SRTM and corrected for the channel slope (2 cm/km).

[b] value per unit km allows comparison between different reaches.

Text DR3. Comparison of our results with the seasonal pattern of suspended sediment discharge by Filizola and Guyot (2009) and Meade (1985), and floodplain sediment budget for the Amazon River reach in between Manacapuru and Obidos compared with Filizola and Guyot (2009).

After calculating the annual washload budget of the four reaches (Fig. 1), we also assessed the seasonal patterns of the washload budget over combined reaches 1-3 (Manacapuru to Obidos). Here we subtracted the combined monthly *Qwl* of the three upstream gauging stations (*MAN*, *FVA*, and *MAO*) from monthly *Qwl* of Obidos (as shown in Fig. 3a and DR11 b). This method is also described in detail in Section 3.2 2nd paragraph. Resulting monthly "net" washload budget (i.e. conceptually an estimation after considering both influx and outflux) is provided in Figs. 3b and DR11 d.

Similar mass balance approach has been used to estimate floodplain sedimentation rates by Filizola and Guyot (2009) using the *Q* and *SSSC* data collected at *MAN* (*SSSC* N=47), *FVA* (N=43), and *OBI* (N=53) during 1980s-2000 (Fig. DR11). They calculated mean monthly *Qwl* and estimated the annual sedimentation budget over the floodplain in the same reach along the Amazon to be around 160 Mt. According to their analysis, however, major loss of washload occurred between March and October, which the period overlaps with the falling phase. We consider our results are relevant due to the following reason. However, our sediment discharge seasonal pattern differs from those by Filizola and Guyot (2009) as presented in figure DR11B. Our results are in general agreement with the relations between suspended sediment discharge and water discharge as earlier postulated by Meade (1985). Most importantly, the period that the net loss of washload over to the floodplain coincide with Q_{rising}, when the river water level rises to make hydrologic connections to floodplain whether through channelized or overbank diffusive flows. Previous studies on sediment budget in the lower Amazon also support our results. For example, Dunne et al. (1998) considered only Q_{rising} in calculating sediment influxes of floodplain in their reach-scale mass balance analysis. Bourgoin et al. (2007) concluded that net sedimentation in the Curuai floodplain is positive only during November to June, i.e. during Q_{rising}. Rudorff et al. (2017)'s hydrodynamic simulation on sediment budget in Curuai Lake also showed that the influx of sediment occurs during the Q_{rising}. We consider that Qwl_{MAN} during $Q_{falling}$ (June-October) by Filizola and Guyot (2009) is overestimated (Figure DR10).. Their results on seasonal patterns at Qwl_{FVA} and Qwl_{OBI} accord with ours.

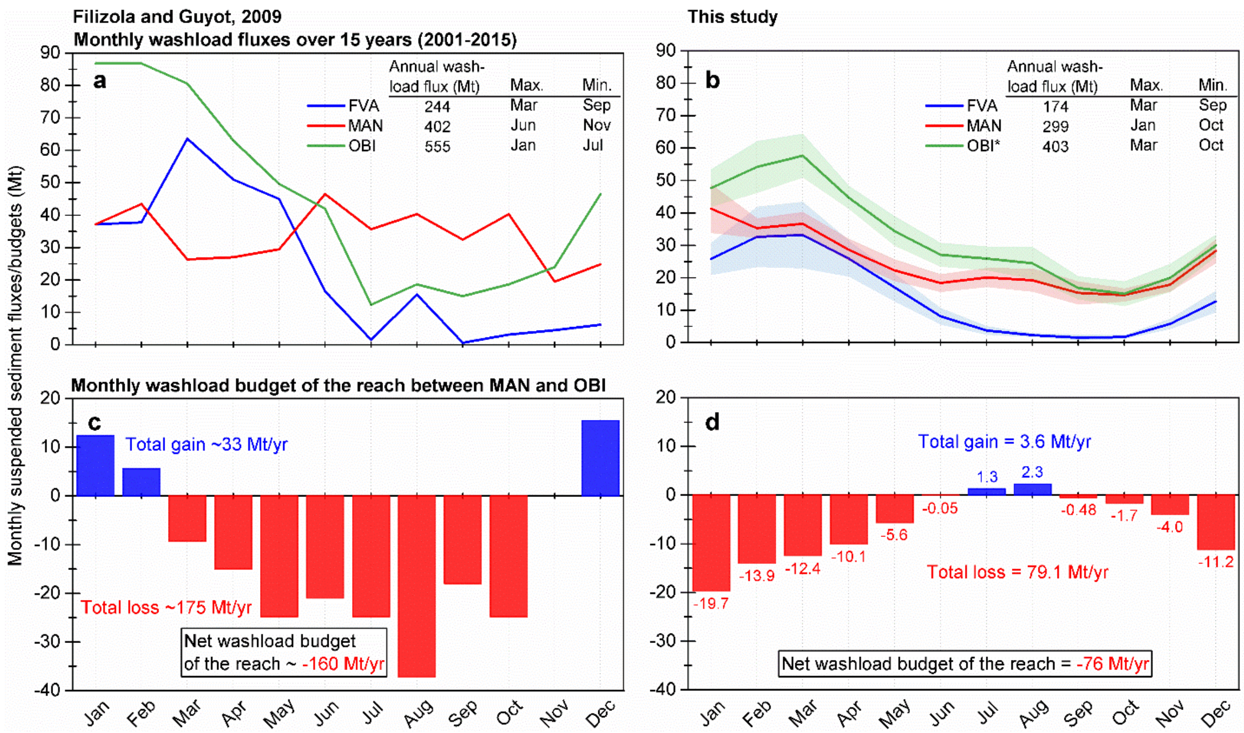

Fig. DR11. Monthly suspended sediment fluxes at FVA, MAN, and OBI gauge stations and its floodplain deposition budget of the reach in between the Madeira confluence and OBI. Results from Filizola and Guyot (2009) (left, a and c) are compared with ours (right, b and d). (a) Mean monthly suspended sediment fluxes and variability at *FVA*, *MAN*, and *OBI* are calculated over 15 years (2001-2014). Monthly net sediment budget of the reach (after interaction with floodplains) in between *MAN* and *OBI* are calculated by differences in their monthly budget. Annual *Qwl* of Negro River at *MAO* (5.4 Mt/yr) (Figure DR1) is included in the calculation.

References Cited

Bouchez, J., Lupker, M., Gaillardet, J., France-Lanord, C., and Maurice, L., 2011, How important is it to integrate riverine suspended sediment chemical composition with depth? Clues from Amazon River depth-profiles: Geochimica et Cosmochimica Acta, v. 75, no. 22, p. 6955-6970,

Bourgoin, L. M., Bonnet, M.-P., Martinez, J.-M., Kosuth, P., Cochonneau, G., Moreira-Turcq, P., Guyot, J.-L., Vauchel, P., Filizola, N., and Seyler, P., 2007, Temporal dynamics of water and sediment exchanges between the Curuaí floodplain and the Amazon River, Brazil: Journal of Hydrology, v. 335, no. 1, p. 140-156, https://doi.org/10.1016/j.jhydrol.2006.11.023

Brierley, G. J., and Fryirs, K. A., 2013, Geomorphology and river management: applications of the river styles framework, John Wiley & Sons.

Constantine, J. A., Dunne, T., Ahmed, J., Legleiter, C., and Lazarus, E. D., 2014, Sediment supply as a driver of river meandering and floodplain evolution in the Amazon Basin: Nature Geoscience, v. 7, no. 12, p. 899-903,

Dunne, T., Mertes, L. A. K., Meade, R. H., Richey, J. E., and Forsberg, B. R., 1998, Exchanges of sediment between the flood plain and channel of the Amazon River in Brazil: Geological Society of America Bulletin, v. 110, no. 4, p. 0450, 10.1130/0016-7606(1998)110<0450:eosbtf>2.3.co;2

Filizola, N., and Guyot, J. L., 2009, Suspended sediment yields in the Amazon basin: an assessment using the Brazilian national data set: Hydrological Processes, v. 23, no. 22, p. 3207-3215, Doi 10.1002/Hyp.7394

Fricke, A. T., Nittrouer, C. A., Ogston, A. S., Nowacki, D. J., Asp, N. E., Souza Filho, P. W., da Silva, M. S., and Jalowska, A. M., 2017, River tributaries as sediment sinks: Processes operating where the Tapajós and Xingu rivers meet the Amazon tidal river: Sedimentology,

Guo, X., 2017, Morphodynamics of large anabranching rivers: the case of the Madeira River, Brazil [Master: University of Texas at Austin.

Huete, A., Didan, K., Miura, T., Rodriguez, E. P., Gao, X., and Ferreira, L. G., 2002, Overview of the radiometric and biophysical performance of the MODIS vegetation indices: Remote Sensing of Environment, v. 83, no. 1, p. 195-213,

Iriondo, M., 1982, Geomorfologia da planície Amazônica: SBG, Simp. Quatern. Brasil, v. 4, p. 323-348,

Kosuth, P., Callede, J., Laraque, A., Filizola, N., Guyot, J. L., Seyler, P., Fritsch, J. M., and Guimaraes, V., 2009, Sea-tide effects on flows in the lower reaches of the Amazon River: Hydrological Processes, v. 23, no. 22, p. 3141-3150, Doi 10.1002/Hyp.7387

Kosuth, P., Vinzon, S., Lima, J., Netto, A., Guyot, J., Dosseto, A., Baume, J., Guennec, B., Filizola, N., and V., G., 2001, Campanha de medições de vazão no rio Amazonas, Manacapuru – Paricatuba – Urucurituba - Obidos Fevereiro – Março de 2001: ANEEL, IRD and HiBAm.

Latrubesse, E. M., 2012, Amazon Lakes, *in* Bengtsson, L., Herschy, R., and Fairbridge, R., eds., Lakes and Reservoirs, Springer Verlag, p. 13-26.

Latrubesse, E. M., Arima, E. Y., Dunne, T., Park, E., Baker, V., d'Horta, F., and others, a., 2017, Damming the rivers of the Amazon Basin: Nature, v. 546, p. 363-369, https://doi.org/10.1038/nature22333

Latrubesse, E. M., and Franzinelli, E., 2002, The Holocene alluvial plain of the middle Amazon River, Brazil: Geomorphology, v. 44, no. 3-4, p. 241-257, Doi 10.1016/S0169-555x(01)00177-5

Latrubesse, E. M., and Park, E., 2017, Rivers and Streams, *in* Marston, R. A., ed., The International Encyclopedia of Geography, John Wiley & Sons, Ltd.

Latrubesse, E. M., and Restrepo, J. D., 2014, Sediment yield along the Andes: continental budget, regional variations, and comparisons with other basins from orogenic mountain belts: Geomorphology, v. 216, p. 225-233,

Latrubesse, E. M., Stevaux, J. C., and Sinha, R., 2005, Tropical rivers: Geomorphology, v. 70, no. 3-4, p. 187-206, DOI 10.1016/j.geomorph.2005.02.005

Martinez, J. M., Guyot, J. L., Filizola, N., and Sondag, F., 2009, Increase in suspended sediment discharge of the Amazon River assessed by monitoring network and satellite data: Catena, v. 79, no. 3, p. 257-264, DOI 10.1016/j.catena.2009.05.011

Meade, R. H., 1985, Suspended sediment in the Amazon River and its tributaries in Brazil during 1982-84: US Geological Survey, 2331-1258.

Meade, R. H., Rayol, J. M., Daconceicao, S. C., and Natividade, J. R. G., 1991, Backwater Effects in the Amazon River Basin of Brazil: Environmental Geology and Water Sciences, v. 18, no. 2, p. 105-114, https://doi.org/10.1007/BF01704664

Mertes, L. A., 1997, Documentation and significance of the perirheic zone on inundated floodplains: Water Resources Research, v. 33, no. 7, p. 1749-1762, https://doi.org/10.1029/97WR00658

Mertes, L. A., Dunne, T., and Martinelli, L. A., 1996, Channel-floodplain geomorphology along the Solimões-Amazon river, Brazil: Geological Society of America Bulletin, v. 108, no. 9, p. 1089-1107, https://doi.org/10.1130/0016-7606(1996)108<1089:CFGATS>2.3.CO;2

Mertes, L. A., and Magadzire, T. T., 2007, Large rivers from space: Large Rivers: Geomorphology and Management, p. 535-552,

Mertes, L. A., Smith, M. O., and Adams, J. B., 1993, Estimating suspended sediment concentrations in surface waters of the Amazon River wetlands from Landsat images: Remote Sensing of Environment, v. 43, no. 3, p. 281-301,

Molinier, M., Guyot, J.-L., De Oliveira, E., Guimarães, V., and Chaves, A., 1995, Hydrologie du bassin de l'Amazone: Proc. Grands Bassins Fluviaux Péri-atlantiques, v. 1, p. 335-344,

Nittrouer, C. A., Kuehl, S. A., Sternberg, R. W., Figueiredo, A. G., and Faria, L. E., 1995, An introduction to the geological significance of sediment transport and accumulation on the Amazon continental shelf: Marine Geology, v. 125, no. 3, p. 177-192,

O'Loughlin, F., Paiva, R., Durand, M., Alsdorf, D., and Bates, P., 2016, A multi-sensor approach towards a global vegetation corrected SRTM DEM product: Remote Sensing of Environment, v. 182, p. 49-59,

Park, E., 2017, Tributary impacts, hydrological connectivity and distribution of sediment sinks in the middle-lower Amazon River [PhD PhD]: University of Texas.

Park, E., and Latrubesse, E. M., 2014, Modeling suspended sediment distribution patterns of the Amazon River using MODIS data: Remote Sensing of Environment, v. 147, p. 232-242, https://doi.org/10.1016/j.rse.2014.03.013

Park, E., and Latrubesse, E. M., 2015, Surface water types and sediment distribution patterns at the confluence of mega rivers: The Solimões-Amazon and Negro Rivers junction: Water Resources Research, v. 51, no. 8, p. 6197-6213, https://doi.org/10.1002/2014WR016757

Park, E., and Latrubesse, E. M., 2017, The hydro-geomorphologic complexity of the lower Amazon River floodplain and hydrological connectivity assessed by remote sensing and field control: Remote Sensing of Environment, v. 198, p. 321-332, https://doi.org/10.1016/j.rse.2017.06.021

Ronchail, J., Guyot, J., Villar, J. C. E., Fraizy, P., Cochonneau, G., De Oliveira, E., Filizola, N., and Ordenez, J. J., 2006, Impact of the Amazon tributaries on major floods at Óbidos: IAHS publication, v. 308, p. 220,

Rudorff, C. M., Dunne, T., and Melack, J. M., 2017, Recent increase of river-floodplain suspended sediment exchange in a reach of the lower Amazon River: Earth Surface Processes and Landforms, v. 43, no. 1, p. 322-332, doi/abs/10.1002/esp.4247

Villar, R. E., Martinez, J. M., Le Texier, M., Guyot, J. L., Fraizy, P., Meneses, P. R., and de Oliveira, E., 2013, A study of sediment transport in the Madeira River, Brazil, using MODIS remote-sensing images: Journal of South American Earth Sciences, v. 44, p. 45-54, DOI 10.1016/j.jsames.2012.11.006